Molecular locking with all-organic surface modifiers enables stable and efficient slot-die-coated methyl-ammonium-free perovskite solar modules

Rana, Prem Jyoti Singh; Febriansyah, Benny; Koh, Teck Ming; Kanwat, Anil; Xia, Junmin; Salim, Teddy; Hooper, Thomas J. N.; Kovalev, Mikhail; Giovanni, David; Aw, Yeow Chong; Chaudhary, Bhumika; Cai, Yongqing; Xing, Guichuan; Sum, Tze Chien; Ager, Joel W.; Mhaisalkar, Subodh Gautam; Nripan, Mathews

2023

Rana, P. J. S., Febriansyah, B., Koh, T. M., Kanwat, A., Xia, J., Salim, T., Hooper, T. J. N., Kovalev, M., Giovanni, D., Aw, Y. C., Chaudhary, B., Cai, Y., Xing, G., Sum, T. C., Ager, J. W., Mhaisalkar, S. G. & Nripan, M. (2023). Molecular locking with all-organic surface modifiers enables stable and efficient slot-die-coated methyl-ammonium-free perovskite solar modules. Advanced Materials. https://dx.doi.org/10.1002/adma.202210176

https://hdl.handle.net/10356/167348

https://doi.org/10.1002/adma.202210176

Molecular Locking with All-Organic Surface Modifiers Enables Stable and Efficient Slot-Die-Coated Methyl-Ammonium-Free Perovskite Solar Modules

Prem Jyoti Singh Rana, Benny Febriansyah, Teck Ming Koh, Anil Kanwat, Junmin Xia, Teddy Salim, Thomas J. N. Hooper, Mikhail Kovalev, David Giovanni, Yeow Chong Aw, Bhumika Chaudhary, Yongqing Cai, Guichuan Xing, Tze Chien Sum, Joel W. Ager, Subodh G. Mhaisalkar, and Nripan Mathews*

P. J. S. Rana, B. Febriansyah, T. M. Koh, A. Kanwat, Y. C. Aw, B. Chaudhary,
S. G. Mhaisalkar, N. Mathews
Energy Research Institute at Nanyang Technological University (ERI@N) Research Techno Plaza
X-Frontier Block Level 5, 50 Nanyang Drive, Singapore 637553,
Singapore
E-mail:nripan@ntu.edu.sg

B. Febriansyah, J.W.Ager
Berkeley Educational Alliance for Research in Singapore (BEARS)Ltd.
1 CREATE Way, Singapore138602,Singapore

J. Xia, Y. Cai, G. Xing
Joint Key Laboratory of the Ministry of Education
Institute of Applied Physics and Materials Engineering
University of Macau
Avenida da Universidade
Taipa, Macau 999078, P. R. China

T. Salim, S. G. Mhaisalkar, N. Mathews
School of Materials Science and Engineering
Nanyang Technological University
Singapore 639798, Singapore

T. J. N. Hooper
Centre of High Field Nuclear Magnetic Resonance (NMR) Spectroscopy and Imaging
Nanyang Technological University
21 Nanyang Link, Singapore 637371, Singapore

M. Kovalev
Cambridge Centre for Advanced Research and Education (CARES)
1 Create way, Singapore 138602, Singapore

D. Giovanni, T. C. Sum
Division of Physics and Applied Physics
School of Physical and Mathematical Sciences
Nanyang Technological University
21 Nanyang Link, Singapore 637371, Singapore

J. W. Ager
Department of Materials Science and Engineering
University of California at Berkeley
Berkeley, CA 94720, USA

Abstract

The power conversion efficiency (PCE) of the state-of-the-art large-area slot-die-coated perovskite solar cells (PSCs) is now over 19%, but issues with their stability persist owing to significant intrinsic point defects and a mass of surface imperfections introduced during the fabrication process. Herein, the utilization of a hydrophobic all-organic salt is reported to modify the top surface of large-area slot-die-coated methylammonium (MA)-free halide perovskite layers. Bearing two molecules, each of which is endowed with anchoring groups capable of exhibiting secondary interactions with the perovskite surfaces, the organic salt acts as a molecular lock by effectively binding to both anion and cation vacancies, substantially enhancing the materials' intrinsic stability against different stimuli. It not only reduces the ingression of external species such as oxygen and moisture, but also suppresses the egress of volatile organic components during the thermal stability testing. The treated PSCs demonstrate efficiency of 19.28% (active area of 58.5 cm^2) and 17.62% (aperture area of 64 cm^2) for the corresponding mini-module. More importantly, unencapsulated slot-die-coated mini-modules incorporating the all-organic surface modifier show ≈80% efficiency retention after 7500 h (313 days) of storage under 30% relative humidity (RH). They also remarkably retain more than 90% of the initial efficiency for over 850 h while being measured continuously.

Introduction

With the efficiencies of perovskite solar cells (PSCs) plateauing at 25%, the focus has turned to the fabrication of long-lasting scaled-up devices.[1] In this regard, slot-die coating technique involving the formation of a stable meniscus and precise control of film thickness has emerged as a front runner owing to its large-area coating uniformity, high-throughput capability, minimal material wastage, as well as compatibility with high volume production.[2] The power conversion efficiency (PCE) of the state-of-the-art slot-die-coated PSCs is now over 20% for small-areas[3] and over 19% for large-areas.[4] These advances are enabled by controlled nucleation and crystal growth of the perovskite via solvent engineering,[4,5] gas or thermal quenching,[6,7] and additives.[8,9] However, there have been very few studies on improving the stability of slot-die-coated devices, especially at the mini-module level (Table S1, Supporting Information).

Most slot-die-coated PSCs utilize methylammonium (MA),[3,5,10–12] which is unstable due to the tendency of the cation to undergo chemistry leading to volatile and electrochemically reactive products.[13–15] More thermally stable formamidinium-cesium (FACs) perovskites [4,7,8,16] are of interest, but they possess different solvation and crystallization characteristics compared to the MA-based systems.[17,18] The low solubility of Cs precursors complicates the crystallization dynamics, leading to the generation of photoinactive $FAPbI_3$ and $CsPbI_3$.[19,20] Furthermore, bromide ions that are typically part of such compositions possess higher diffusivity and lower solubility in the organic solvent, making the deposition of high-quality FACs perovskites over the large area even more difficult to control.[7,8,21] Consequently, the resulting films suffer from significant intrinsic point defects [22] and a mass of surface imperfections.[23]

Owing to the diversity of the surface defects, limitations exist in the use of the previously reported passivators with most of them being able to passivate only one or two kinds of trap states. Neutral Lewis bases, like *n*-trioctylphosphine oxide [24] can passivate undercoordinated Pb ions, but not charged defects. Ammonium-based halide salts can neutralize the surface ionic defects, but many of them tend to induce the formation of resistive low-dimensional species.[25–27] Halide counterions are also prone to oxidation and diffusion.[28–30] As variation of crystallization kinetics and the presence of residual solvents can become more significant in large-area coating, there is, therefore, an urgent need for the development of new passivation approaches capable of addressing a wide variety of defects.

Result and Discussion

All-organic passivators are a new paradigm since they provide a facile and fertile playground for tailoring steric and electronic properties through a combination of rational design, structural functionalization, and chemical synthesis. Such flexibility allows desired properties to be augmented in a single passivator moiety (i.e., molecular engineering) so that the stability and efficiency of FACs perovskites can be improved. In this work, we introduce an all-organic passivator, represented by fluorinated anilinium benzylphosphonate, (denoted as FABP; Figure 1a), to substantially enhance the FACs perovskite's moisture, thermal and electrical stabilities. Endowed with both ammonium and phosphonate groups, FABP acts as an effective defect passivator and ion migration inhibitor by binding to the FA-site vacancy, while concurrently addressing the undercoordinated Pb2+.

While solid-state nuclear magnetic resonance (ss-NMR) spectroscopy confirmed the presence of secondary interaction between FABP and the perovskite (in the form of ionic and hydrogen bonding interactions), density functional theory (DFT) calculations verified the capability of FABP in binding with the possible surface imperfections, thus passivating the defect sites. Proton transfer reaction-mass spectroscopy (PTR-MS) indicated that bonding with FABP retards perovskite degradation under thermal stress. The effectiveness of the broad defect passivator was further demonstrated by their utilization in large-area devices. Slot-die-coated $FA_{0.85}Cs_{0.15}PbI_{2.87}Br_{0.13}$ mini-modules with FABP post-treatment demonstrate PCEs of 19.28% (for an active area of 58.5 cm^2) and 17.62% (aperture area of 64 cm^2). Unencapsulated FABP-based devices show excellent thermal stability, retaining 80% and 70% of its initial PCEs after 2700 and 1700 h at 65 and 85 °C, respectively. Unencapsulated FABP-based minimodules show ≈80% efficiency retention after 7500 h (313 days) under 30% relative humidity (RH). They also remarkably retain more than 90% of the initial efficiency for over 850 h while being measured continuously under light illumination. The testing at 85 °C was conducted on the encapsulated device to minimize the impact caused by dopants used in the Spiro-OMeTAD layer as FACs perovskite is known to be intrinsically stable within this temperature range.

The MA-free perovskite composition used in this work, $Cs_{0.15}FA_{0.85}Pb(I_{083}Br_{0.17})_3$, is relatively stable toward heat stress (85 °C) under inert atmosphere (Figure S1, Supporting Information), but drastic degradation was observed in ambient (Figure S2, Supporting Information). On the contrary, FABP passivated samples showed significant improvement in thermal stability, especially under high relative humidity conditions. Optical absorption measurements of control devices under thermal stress revealed a significant reduction in the main absorption peak at ≈737 nm along with the appearance of the PbI_2 absorption peak at 510 nm after 400 h of testing at 85 °C/75% RH (Figure 1b; Figure S2e, Supporting Information). On the other hand, there is no significant PbI_2 peak detected for passivated films even after 840 h under the same exposure conditions (Figure 1b; Figure S2e, Supporting Information). This can be attributed to the hydrophobicity of FABP passivated layers due to their fluorinated nature and strong bonding with the perovskite surface (Figure S2f, Supporting Information; vide infra).

In situ grazing-incidence X-ray diffraction (GI-XRD) measurements conducted during the thermal aging at 85 °C (Figure 1c; Figure S3, Supporting Information) further corroborated the absorbance data. The constant evolution from perovskite to PbI_2 at elevated temperature implies that FA cations could still thermally decompose, but the application of an FABP overlayer is capable of considerably abating the associated process. To verify, we performed PTR-MS measurement (Figure S4, Supporting Information) on the control and passivated samples. At high temperatures, ammonia (NH_3) and putative triazine ($C_3H_3N_3$) are the main thermal decomposition products of FACs perovskite (Figure 1d,e; Figure S4, Scheme S1a,b, Supporting Information). As temperature increases, the triazine and ammonia intensities were found to be higher for the control sample than that for the passivated sample. Thus, the presence of FABP layer not only reduces the ingression of ambient (that could lead to degradation) but also suppresses the loss of the volatile organic components during thermal stress.

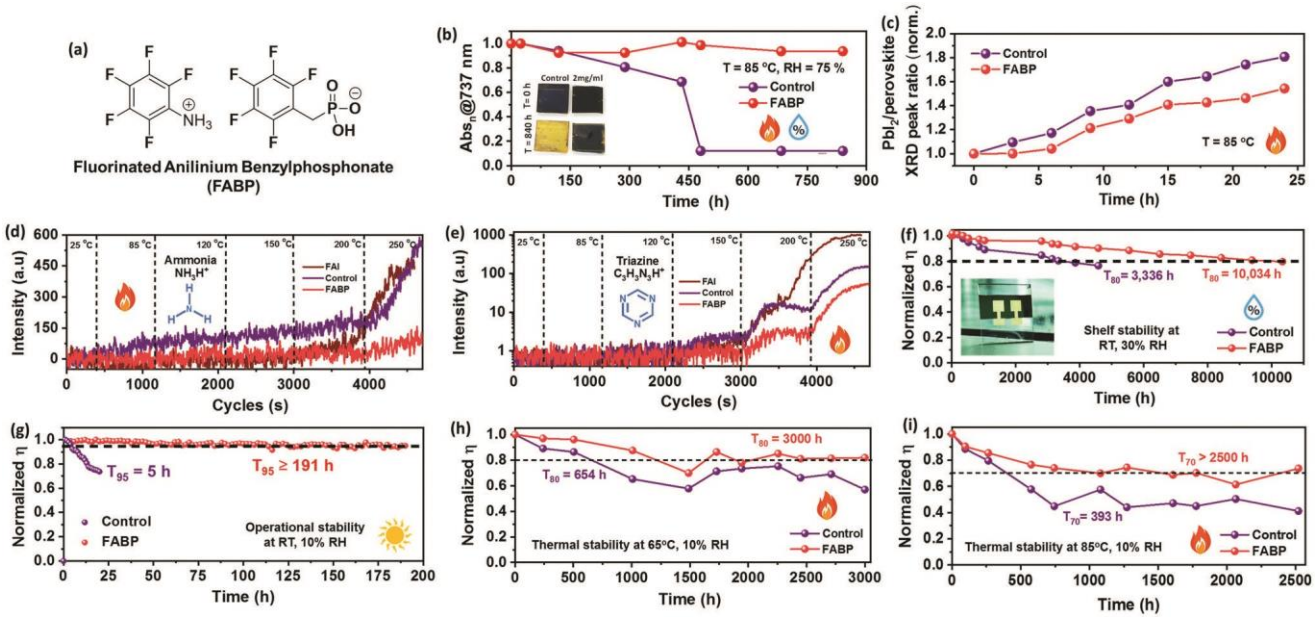

Figure 1. Effect of FABP on intrinsic stability of halide perovskites. a) Molecular structure of all-organic surface passivator FABP. b) Normalized absorbance values as a function of the aging time (stored at T = 85 °C and 75% RH) for control and FABP-treated films (2 mg mL^{-1}). c) Normalized ratio between the PbI_2 (2θ=12.7°) and the main 3D perovskite diffraction peak (2θ= 14.2°) intensities, for control and FABP-treated films. d,e) Time dependence of ammonia (NH_3) (d) and triazine ($C_3H_3N_3$) (e) outgasses extracted from PTR-MS spectra of FAI, control, and FABP-treated films. f) Shelf stability for unencapsulated solar cells stored in the dark at room temperature with RH of 30% over 10 000 h. g) Operational stability at initial maximum power point (MPPT) condition for unencapsulated solar cells measured under continuous illumination in dry air for almost 200 h. h) Thermal stability of solar cells at 65 °C monitored over 3000 h (unencapsulated). i) Thermal stability of control and FABP-treated PSCs at 85 °C monitored over 2500 h (PIB-based blanket encapsulation).

PSCs with an n–i–p structure of FTO/SnO_2/perovskite/SpiroOMeTAD/Au were constructed to assess the efficiency and durability of the corresponding devices under different conditions. The PCEs (≈0.09 cm^2 area) are typically in the range of 16–18% for the control and 18–20% for the passivated devices with almost negligible hysteresis (vide infra). As shown in Figure 1f, passivated devices (unencapsulated) show impressively high shelflife stability, retaining ≈80% of its initial PCE after 418 days (10 034 h) in 30% RH, whereas the control devices dropped to ≈80% after only 139 days (3336 h). Passivated devices tested under continuous one sun illumination (<10% RH) were able to provide 95% of its original power output for over 190 h (unencapsulated), while the corresponding value was only 5 h for the control devices (Figure 1g). Long-term thermal stability investigation of the devices with the same architecture was also performed at 65 °C (unencapsulated) and 85 °C (encapsulated) under 10% RH. As depicted in Figure 1h,i, under all conditions, passivated devices outperformed the control devices, retaining ≈80% of its initial PCE after 3000 h at 65 °C and ≈70% of its initial PCE after more than 2500 h at 85 °C (Figures S5–S8, Supporting Information).

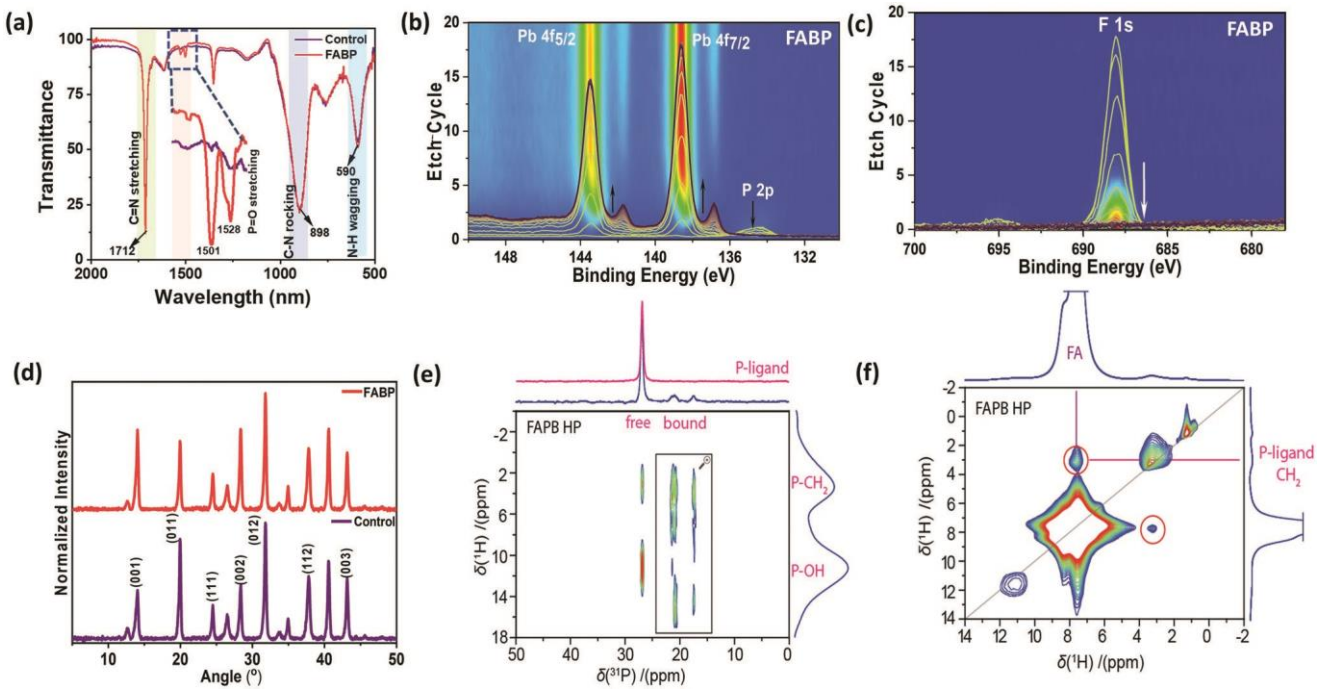

Figure 2. Presence and interaction of FABP passivator with halide perovskite. a) IR spectra of control and FABP-treated perovskite films. b,c) Depthprofiling XPS spectra showing the evolution of Pb 4f, P 2p, and F 1s core levels with etching cycles (60 s cycle^{-1}) of FABP-treated films. d) Grazing -incidence XRD of control and FABP-treated films. e,f) ^{31}P–^{1}H 2D NMR HETCOR and ^{1}H–^{1}H NOESY spectra of FABP-treated films.

To unravel the reasons behind the improved stability, we further probed the interaction between the passivator and the perovskite layer as well as its impacts on the resulting material's morphological, structural, and optoelectronic qualities. Fourier transform infrared (FTIR) spectroscopy and depth-profiling Xray photoelectron spectroscopy (XPS) measurements indicate the presence of the organic species only on the top surface of the film (**Figure 2**a–c; Figures S9 and S10, Table S2, Note S1, Supporting Information). Grazing-angle X-ray diffractograms of perovskite films treated with FABP indicate no traces of electrically resistive low-dimensional perovskite peaks (Figure 2d), suggesting that the organic molecules just passivate the surfaces of the 3D perovskite crystallites.[31] Ss-NMR spectroscopy further confirms that the organic salts interact with the perovskite surface at the molecular level via hydrogen bonding (see Note S2, Supporting Information for further discussion). In particular, the ^{31}P–^{1}H 2D heteronuclear correlation (HETCOR) spectrum of the FABP-treated sample reveals correlations between ^{31}P and ^{1}H environments, indicating that they are spatially close with each other, with the bound P-ligand environments exhibiting a more downshifted ^{1}H frequency (15.0 ppm) relative to the free ligand (11.3 ppm) (Figure 2e). The ^{1}H–^{1}H 2D nuclear Overhauser effect spectroscopy (NOESY) spectrum also shows correlation resonances in the form of cross-peaks between the ^{1}H resonances of the HP FA cation and the P-ligand CH_2 group, confirming that these environments are near in space and that the P-ligand is bonded to the perovskite surface (Figure 2f).

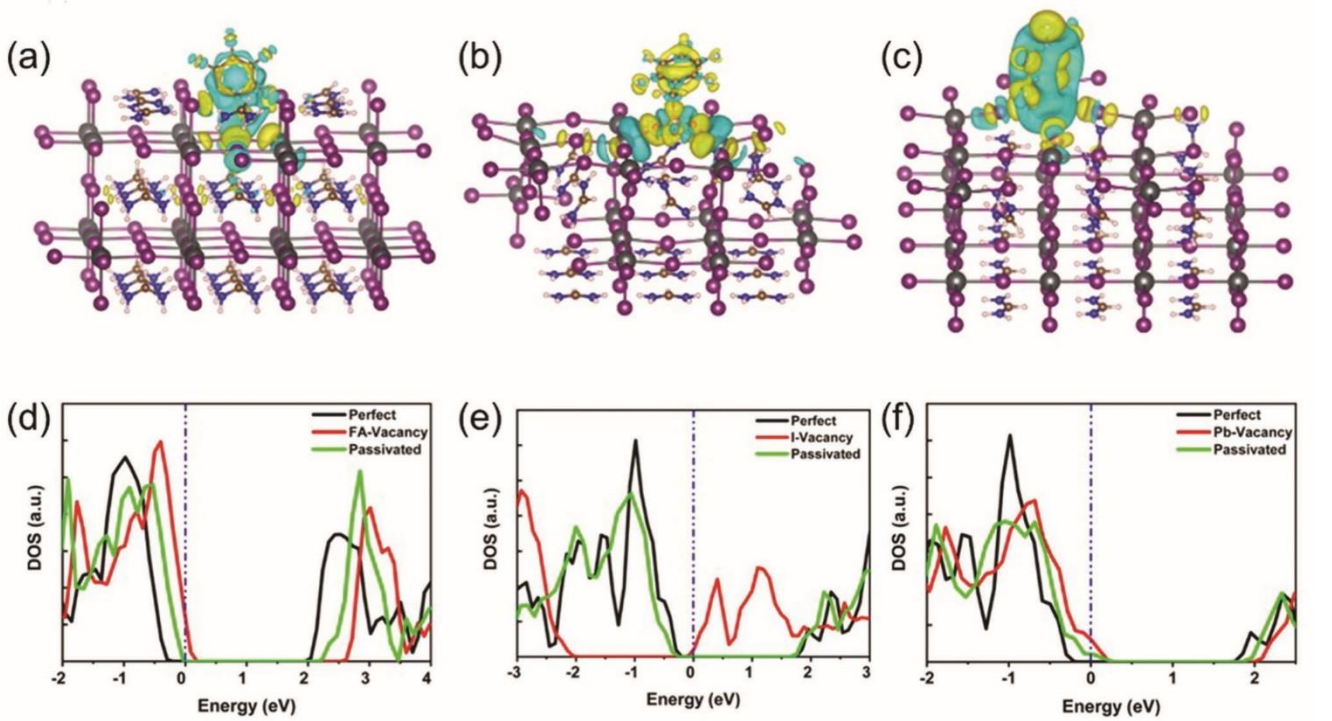

Figure 3. DFT calculations of FABP-treated films. a–c) The yellow (cyan) color represents charge accumulation (losses) of the $FAPbI_3$ surface with FA vacancy passivated by pentafluoroanilinium cation (a); I vacancy passivated by pentafluorobenzyl phosphonate anion (b); Pb vacancy passivated by pentafluoroanilinium cation (c). d–f) The total density of states (DOS) of $FAPbI_3$ with FA vacancy, pentafluoroanilinium-passivated, and a perfect crystal (d); with I-defect, pentafluorobenzyl-phosphonate-passivated, and a perfect crystal (e); with Pb-defect, pentafluoroanilinium-passivated, and a perfect crystal (f). The dotted blue line represents the *E*-Fermi level for each of the scenarios.

Density functional theory (DFT) calculations were performed using the Vienna Ab initio Simulation Packages (VASP) with the generalized gradient approximation (GGA) to understand the impact of each organic component of FABP on the defect passivation pathway.[32–34] Ab initio molecular dynamics simulation of the structures indicate that the passivator molecules could adsorb well on the surface of the defective $FAPbI_3$ surface (**Figure 3**a–c). $FAPbI_3$ was utilized as a simplified model due to the similarity of its structure to our composition.[20,35] First principles density functional theory (DFT) calculations on several ionic defects such as FA^+ vacancies (V_{FA}), I^- vacancies (V_I), and Pb^{2+} vacancies (V_{Pb}) in $FAPbI_3$ confirms that such adsorption process leads to a passivation effect (see Note S3 and Figures S11–S15, Supporting Information) for more details). In particular, differential charge density distributions and electron localization function results indicate the presence of electron transfer and delocalization between the FABP molecules and the vacancies, leading to the formation of new interaction and bonding. This is possible owing to the ammonium and phosphonate functionalities within the organic passivator that are capable of addressing the defects (pentafluoroanilinium with V_{FA} and V_{Pb}, while pentafluorobenzyl phosphonate with V_I; Figure S14a–f, Supporting Information). Density of state (DOS) calculations indicate Fermi level shifts back to the perovskite bandgap on binding with both the pentafluoroanilinium and pentafluorobenzyl phosphonate species (Note S3, Supporting Information), highlighting the effectiveness of our molecule in passivating various surface trap states. Based on the Bader charge calculation, it is revealed that the O atoms on the pentafluorobenzyl phosphonate molecule have more electrons than other phosphonate molecules based on different backbones (Table S3 and Figure S15c–f, Supporting Information), suggesting that the fully fluorinated benzene core provides a more efficient coordination ability with the vacancies. This underlines the importance of the rational design of functional group to enhance the interaction with the vacancy on the perovskite surfaces.

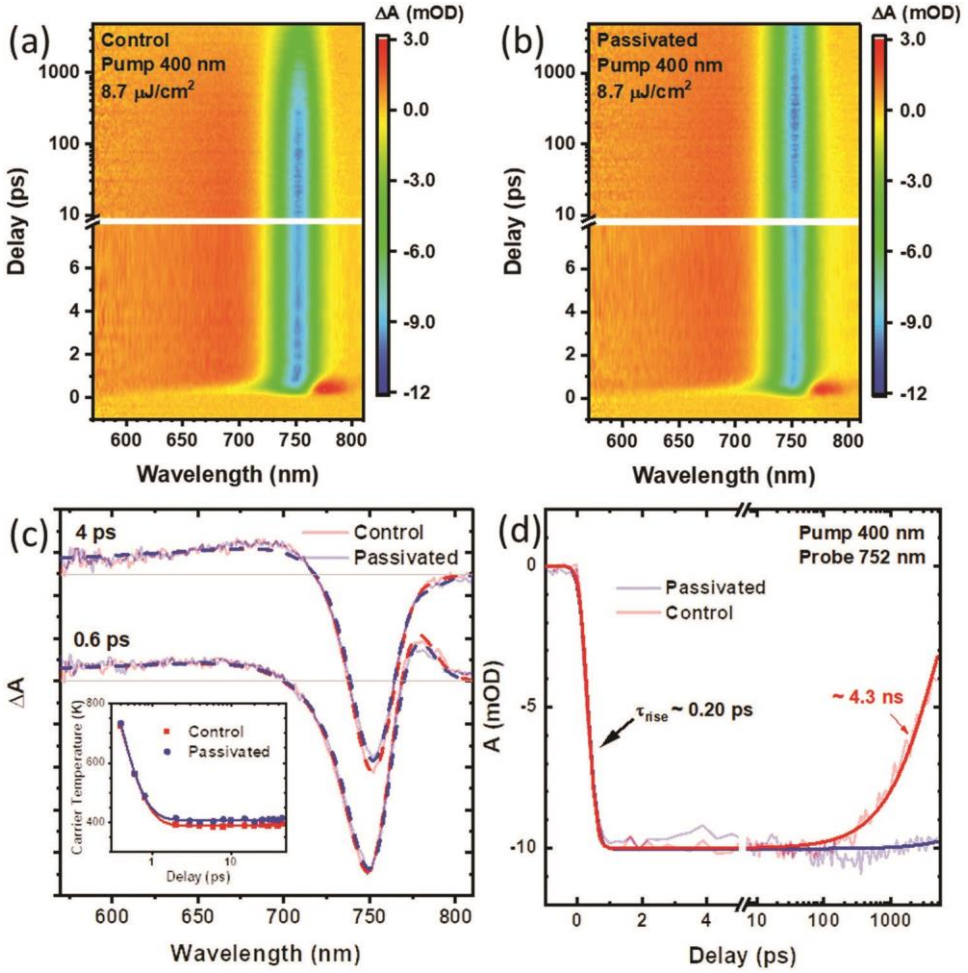

Figure 4. TA spectra of perovskite films. a,b) Pseudocolour TA plots for the control (a) and passivated (b) perovskite films. c) Comparison of the TA spectra features at 0.6 and 4.0 ps for both samples—photobleaching (PB) minima ($\Delta A < 0$) at ≈750 nm and photoinduced absorption (PIA) band ($\Delta A > 0$) for wavelengths below 700 nm. Inset: Carrier cooling dynamics obtained from TA model fitting.[38] d) TA kinetics of the control and passivated films at the PB minima (≈750 nm).

Transient absorption (TA) measurements were conducted to investigate the photoexcitation dynamics up to the first few ns of our perovskite samples with and without a passivator. **Figure4**a,b shows the pseudocolor TA plots for the control and passivated samples, respectively. As expected, a clear photobleaching minima (PB, $\Delta A < 0$) is present at ≈750 nm, which corresponds to the band-edge population .[36] Beside the PB peak, a broad photoinduced absorption (PB, $\Delta A > 0$) band at shorter wavelengths (i.e., <≈700 nm) is also observed, which is assigned to a combination of bandgap renormalization and excited state absorption[37] (see Figure 4c). At early time, up to several ps, there is no observable difference in the PB rise time ($\tau_{rise} \approx 0.2$ ps) of both samples (Figure 4d). Similar carrier cooling dynamics is also observed for both samples, obtained from our TA model fitting (Figure 4c inset).[38] These observations imply that the passivation has no effect on hot-carrier cooling (i.e., carrier–phonon interactions). However, one notable change due to the passivation is the carrier lifetime lengthening from 4.3 ± 0.1 ns to a much longer timescale beyond our measurement range (Figure 4d). This indicates the FABP treatment significantly cuts down the undesirable trap-assisted recombination. Consistent with the TA result, passivated films exhibited higher photoluminescence quantum yields (PLQYs) and more stable PL emission (Figure S16, Supporting Information) as compared to the control film. Moreover, the passivation effect is also clear in electroluminescence (EL) measurements under different biases. The emission from passivated layer is stable and no EL peak shift with increasing bias from 1.2 to 2.7 V is observed (Figure S17, Supporting Information).

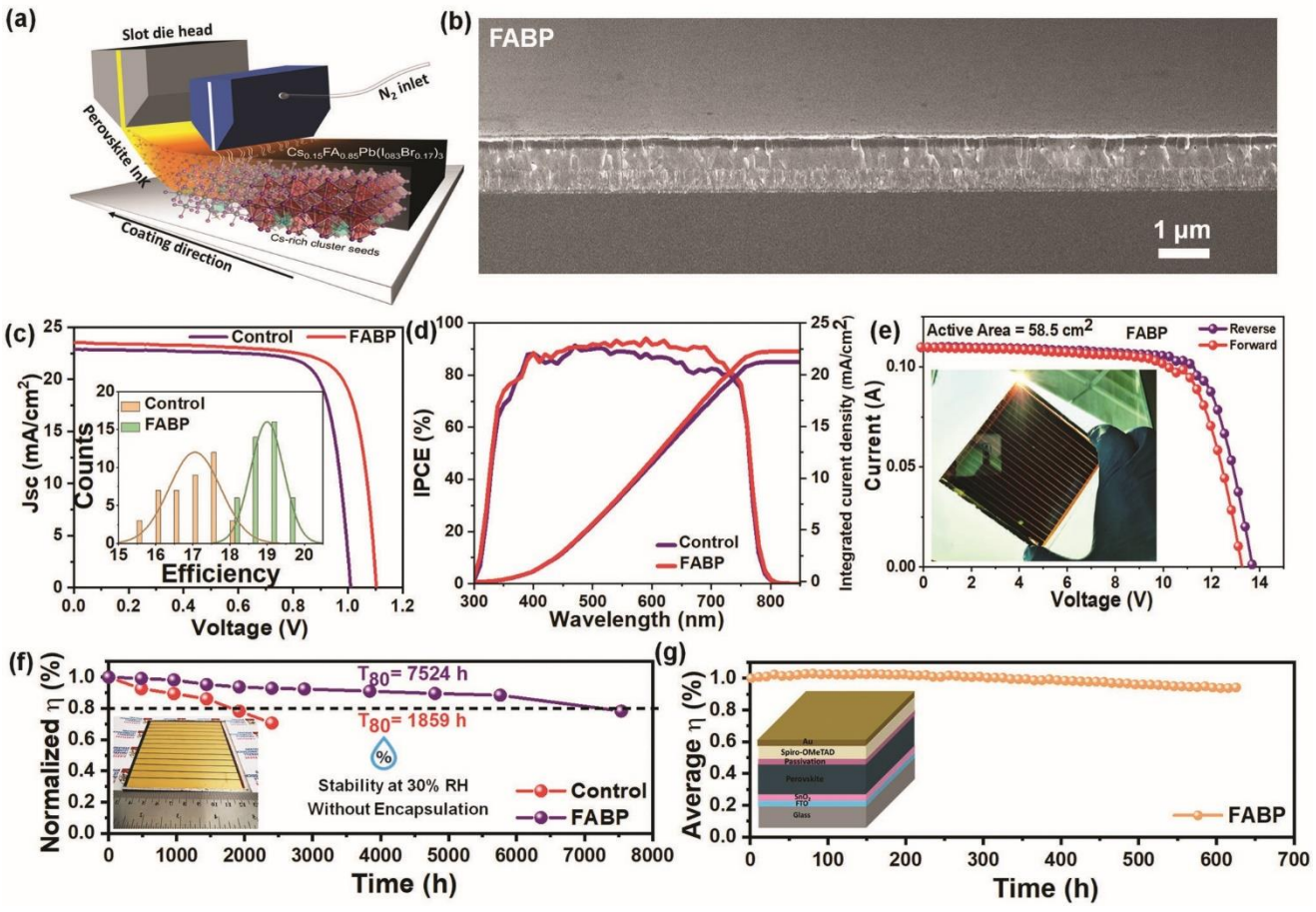

Figure 5. Photovoltaic performance and stability of slot-die coated perovskite devices. a) Schematic illustration for N_2-knife- and heat-assisted slot-die coating of perovskite films. b) Cross-sectional SEM images of FABP-treated perovskite devices. c) *J-V* curves of the small-area champion devices. Inset: Statistical PCE results of 40 devices from each batch. d) EQE spectra with integrated J_{sc} curve of control and FABP-treated PSCs. e) *J–V* curve of the best performing passivated perovskite solar modules (PSMs) (inset: PSM with 13 sub-cells). f) Shelf stability for unencapsulated PSMs stored in the dark at room temperature with RH of 30% over 7500 h. g) Operational stability of unencapsulated FABP-treated PSM measured under continuous illumination in dry air environment for almost 900 h.

All of the experimental results discussed above were conducted on slot-die coated samples where homogeneous perovskite coating over a large substrate could be achieved (Figure 5a). Morphologically, the passivated perovskite films feature similar grain sizes (Figure S18, Supporting Information) and surface roughness as the control sample (FigureS19, Supporting Information),which corroborate the previous XPS and GI-XRD results that indicated how the all-organic FABP does not induce reconstruction or recrystallization of the 3D perovskite. The cross-sectional FESEM images depicted in Figure 5b and Figure S20 (Supporting Information) further show that compact and uniformly covered perovskite films are realized with an average film thickness of approximately 600 nm. Small PSCs in n–i–p configuration (FTO/SnO2/perovskite with or without FABP/Spiro-OMeTAD/Au) were fabricated from a 100 cm2 perovskite film coated on FTO/SnO2 substrate (see Supporting Information for fabrication details). Current density–voltage (J−V) curves of PSCs with various passivator concentration (0 to 10 mg mL−1) were then recorded with 2 mg mL−1 of passivator showing the optimized high-efficiency device performance.

Their related photovoltaic data are summarized in Table S5 (Supporting Information). The J–V curves of the champion devices of control and different FABP-treated PSCs are shown in Figure 5c. The control device shows PCE of 18.15% (with short circuit current density (Jsc) = 22.86 mA cm−2, open-circuit voltage (Voc) = 1.00 V, and fill factor (FF) = 0.79) while the passivated PSCs show PCE of 19.95% (with Jsc = 23.56 mA cm−2, Voc = 1.09 V, and FF = 0.77) (active area of 0.09 cm2). To the best of our knowledge, 19.95% is among the highest efficiency for passivated small area perovskite solar cells using the one-step slot-die coating technique (see Tables S6 and S7, Supporting Information for comparison with other reported slot-die coated devices). Our passivation approach offers PCE enhancement of almost two absolute percent which is mainly attributed to the significantly increased Voc from 1.00 to 1.10 V.

In agreement with UV–vis and PL analysis (Figure S21a.b, Supporting Information), no shift in the onset of the incident photon-to-electron conversion efficiency (IPCE) spectra (Figure 5d; Figure S21c, Supporting Information) was detected. The integrated Jsc for control and passivated PSC are 21.23 and 22.41 mA cm−2 respectively, which is within ± 5% deviation from the Jsc recorded from the J−V measurement. Notably, the passivated PSC possesses higher quantum efficiency in the range from 500–775 nm due to better interface and efficient charge carrier extraction at the perovskite/HTM interface. The passivated PSCs show high device performance with narrower efficiency distribution and higher reproducibility (inset of Figure 5c; Figure S22, Supporting Information). Overall, the average PCE of control and passivated devices are 17.40% and 19.00% respectively (40 devices each). We observed a negligible hysteresis in passivated devices, which indicates a significant decrease in the defect and/or traps at the interface (Figure S23, Supporting Information).[39,40] To demonstrate the universality of our molecularly-designed all-organic salt in improving the device's performance, we also investigated spin-coated FACs-based perovskite (Figure S24, Supporting Information). To probe the influence of the organic functionality, we further examined passivators without fluorination (anilinium benzyl phosphonate (ABP)) and with alternative binding group (anilinium benzyl carboxylate -ABC). FABP-based devices outperformed the other passivators based on superior Voc and Jsc, highlighting the judicious design of the molecule.

Finally, large-area mini-modules consisting of 13 cells connected in series (over 100 cm2 conducting glass substrates) were fabricated (Figure S25a–c, Supporting Information). The best performing perovskite solar module (PSM; active area of 58.5 cm2) showed PCEs of 19.28% (Voc 13.70 V, Isc 0.109 A and FF of 75.04%) Figure 5e; Table S8, Supporting Information), performing better than the control mini-modules which showed a PCE of 15.05% (Voc 13.82 V, Isc 0.102 A and FF of 61.11%; Figure S25d, Supporting Information). The FABP passivated perovskite solar mini module (unencapsulated) demonstrated outstanding stability under 30% RH (Figure 5f), maintaining ≈80% of its initial PCE even after ≈313 days (7524 h), while the control mini-module retained a similar magnitude of performance only for ≈77 days (1859 h). Impressively the FABP-treated PSMs retained more than 90% of the initial efficiency after more than 850h of exposure at continuous one sun illumination(Figure5g), attesting to the effectiveness of this new generation of non halide based passivator in boosting the stability of perovskites via the strong binding and secondary interaction between both organic molecules and perovskite surfaces.

Conclusion

We have demonstrated the design and utilization of new all organic salts as effective surface-modifying agents to improve the quality of large-area slot-die-coated FACs perovskite layers. Represented by hydrophobic fluorinated anilinium benzyl phosphonate (FABP),various characterization techniques confirm the role of the participating ionic molecules in both passivating the defects and abating ion migration within the perovskite surfaces. Such effects are achieved as a result of intermolecular interactions of the organic species with FA-site vacancy and undercoordinated Pb ions, which in turn is realized through incorporation of suitable anchoring functional groups in the organic backbone. In comparison to the control (pristine) devices, treatment with the organic salts resulted in PSCs that feature not only superior power conversion efficiencies, but also enhanced stability profiles against different stimuli, such as moisture, oxygen, and heat. Our work points ot the importance of molecular engineering in developing novel effective surface modifiers for efficient and stable PSCs.

Acknowledgements

The authors would like to acknowledge funding from the Singapore National Research Foundation through the Intra-CREATE Collaborative Grant (NRF2018-ITC001-001), Competitive Research Program (CRP) (NRFCRP25-2020-0002), NRF Investigatorship (NRF-NRFI-2018-04), MOE Tier 2 project MOE2019-T2-2-097, and the Science and Technology Development Fund, Macao SAR (File no. 0082/2021/A2). Calculation work was performed in part at the High-Performance Computing Cluster (HPCC), which was supported by the Information and Communication Technology Office (ICTO) of the University of Macau.

Conflict of Interest

The authors declare no conflict of interest.

Author Contributions

P.J.S.R. and B.F. contributed equally to this work. P.J.S.R. and B.F. conceived the idea and wrote the first draft of the manuscript. P.J.S.R., B.F., and Y.C.A fabricated both perovskite solar cells and mini-modules, conducted shelf- and thermal-stability tests, and analyzed the results. T.M.K., S.M., and N.M. contributed to experimental plans and data interpretation. A.K. carried out FTIR, PLQY, LED, and XRD measurements, J.X., Y.C., and G.X conducted theoretical calculations and analysis, B.C. performed thermal in situ XRD measurement, T.S. performed XPS measurement and discussion, T.J.N.H. carried out NMR measurement and analysis, M.K. conducted PTR-MS measurement and data interpretation, D.G. and T.C.S. contributed to TA experiments and analysis. J.W.A., S.M., and N.M. coordinated and directed the work. N.M., B.F., P.J.S.R., and T.M.K. finalized the submitted version of the manuscript with input from all authors.

References

[1] N.-G. Park, K. Zhu, *Nat. Rev. Mater.* **2020**, *5*, 333.
[2] R. Patidar, D. Burkitt, K. Hooper, D. Richards, T. Watson, *Mater. Today Commun.* **2020**, *22*, 100808.
[3] J. Li, J. Dagar, O. Shargaieva, M. A. Flatken, H. Köbler, M. Fenske, C. Schultz, B. Stegemann, J. Just, D. M. Többens, A. Abate, R. Munir, E. Unger, *Adv. Energy Mater.* **2021**, *11*, 2003460.
[4] T. Bu, J. Li, H. Li, C. Tian, J. Su, G. Tong, L. K. Ono, C. Wang, Z. Lin, N. Chai, X.-L. Zhang, J. Chang, J. Lu, J. Zhong, W. Huang, Y. Qi, Y.-B. Cheng, F. Huang, *Science* **2021**, *372*, 1327.
[5] B. Dou, J. B. Whitaker, K. Bruening, D. T. Moore, L. M. Wheeler, J. Ryter, N. J. Breslin, J. J. Berry, S. M. Garner, F. S. Barnes, S. E. Shaheen, C. J. Tassone, K. Zhu, M. F. A. M. Van Hest, *ACS Energy Lett.* **2018**, *3*, 2558.

[6] J.-E. Kim, Y.-S. Jung, Y.-J. Heo, K. Hwang, T. Qin, D.-Y. Kim, D. Vak, *Sol. Energy Mater. Sol. Cells* **2018**, *179*, 80.
[7] M. Fievez, P. J. Singh Rana, T. M. Koh, M. Manceau, J. H. Lew, N. F. Jamaludin, B. Ghosh, A. Bruno, S. Cros, S. Berson, S. G. Mhaisalkar, W. L. Leong, *Sol. Energy Mater. Sol. Cells* **2021**, *230*, 111189.
[8] Z. Yang, W. Zhang, S. Wu, H. Zhu, Z. Liu, Z. Liu, Z. Jiang, R. Chen, J. Zhou, Q. Lu, Z. Xiao, L. Shi, H. Chen, L. K. Ono, S. Zhang, Y. Zhang, Y. Qi, L. Han, W. Chen, *Sci. Adv.* **2021**, *7*, eabg3749.
[9] P. J. S. Rana, B. Febriansyah, T. M. Koh, B. T. Muhammad, T. Salim, T. J. N. Hooper, A. Kanwat, B. Ghosh, P. Kajal, J. H. Lew, Y. C. Aw, N. Yantara, A. Bruno, S. A. Pullarkat, J. W. Ager, W. L. Leong, S. G. Mhaisalkar, N. Mathews, *Adv. Funct. Mater.* **2022**, *32*, 2113026.
[10] D. Burkitt, R. Patidar, P. Greenwood, K. Hooper, J. Mcgettrick, S. Dimitrov, M. Colombo, V. Stoichkov, D. Richards, D. Beynon, M. Davies, T. Watson, *Sustainable Energy Fuels* **2020**, *4*, 3340.
[11] E. Bi, W. Tang, H. Chen, Y. Wang, J. Barbaud, T. Wu, W. Kong, P. Tu, H. Zhu, X. Zeng, J. He, S.-I. Kan, X. Yang, M. Grätzel, L. Han, *Joule* **2019**, *3*, 2748.
[12] S.-H. Huang, C.-K. Guan, P.-H. Lee, H.-C. Huang, C.-F. Li, Y.-C. Huang, W.-F. Su, *Adv. Energy Mater.* **2020**, *10*, 2001567.
[13] D. P. Mcmeekin, G. Sadoughi, W. Rehman, G. E. Eperon, M. Saliba, M. T. Hörantner, A. Haghighirad, N. Sakai, L. Korte, B. Rech, M. B. Johnston, L. M. Herz, H. J. Snaith, *Science* **2016**, *351*, 151.
[14] S.-H. Turren-Cruz, A. Hagfeldt, M. Saliba, *Science* **2018**, *362*, 449.
[15] B. Conings, J. Drijkoningen, N. Gauquelin, A. Babayigit, J. D'haen, L. D'olieslaeger, A. Ethirajan, J. Verbeeck, J. Manca, E. Mosconi, F. D. Angelis, H.-G. Boyen, *Adv. Energy Mater.* **2015**, *5*, 1500477.
[16] Y. Sha, E. Bi, Y. Zhang, P. Ru, W. Kong, P. Zhang, X. Yang, H. Chen, L. Han, *Adv. Energy Mater.* **2021**, *11*, 2003301.
[17] J.-W. Lee, Z. Dai, C. Lee, H. M. Lee, T.-H. Han, N. De Marco, O. Lin, C. S. Choi, B. Dunn, J. Koh, D. Di Carlo, J. H. Ko, H. D. Maynard, Y. Yang, *J. Am. Chem. Soc.* **2018**, *140*, 6317.
[18] J. Xu, C. C. Boyd, Z. J. Yu, A. F. Palmstrom, D. J. Witter, B. W. Larson, R. M. France, J. Werner, S. P. Harvey, E. J. Wolf, W. Weigand, S. Manzoor, M. F. A. M. V. Hest, J. J. Berry, J. M. Luther, Z. C. Holman, M. D. McGehee, *Science* **2020**, *367*, 1097.
[19] J.-W. Lee, D.-H. Kim, H.-S. Kim, S.-W. Seo, S. M. Cho, N.-G. Park, *Adv. Energy Mater.* **2015**, *5*, 1501310.
[20] L. T. Schelhas, Z. Li, J. A. Christians, A. Goyal, P. Kairys, S. P. Harvey, D. H. Kim, K. H. Stone, J. M. Luther, K. Zhu, V. Stevanovic, J. J. Berry, *Energy Environ. Sci.* **2019**, *12*, 1341.
[21] Y. Galagan, F. Di Giacomo, H. Gorter, G. Kirchner, I. De Vries, R. Andriessen, P. Groen, *Adv. Energy Mater.* **2018**, *8*, 1801935.
[22] J. M. Ball, A. Petrozza, *Nat. Energy* **2016**, *1*, 16149.
[23] B. Chen, P. N. Rudd, S. Yang, Y. Yuan, J. Huang, *Chem. Soc. Rev.* **2019**, *48*, 3842.
[24] D. W. Dequilettes, S. Koch, S. Burke, R. K. Paranji, A. J. Shropshire, M. E. Ziffer, D. S. Ginger, *ACS Energy Lett.* **2016**, *1*, 438.
[25] T. M. Koh, V. Shanmugam, X. Guo, S. S. Lim, O. Filonik, E. M. Herzig, P. Müller-Buschbaum, V. Swamy, S. T. Chien, S. G. Mhaisalkar, N. Mathews, *J. Mater. Chem. A* **2018**, *6*, 2122.
[26] Y. Liu, S. Akin, L. Pan, R. Uchida, N. Arora, J. V. Milic, A. Hinderhofer, F. Schreiber, A. R. Uhl, S. M. Zakeeruddin, A. Hagfeldt, M. I. Dar, M. Grätzel, *Sci. Adv.* **2019**, *5*, eaaw2543.
[27] S. Jeong, S. Seo, H. Yang, H. Park, S. Shin, H. Ahn, D. Lee, J. H. Park, N.-G. Park, H. Shin, *Adv. Energy Mater.* **2021**, *11*, 2102236.
[28] J. Joseph Yeow Wan Foong, B. Febriansyah, P. Jyoti Singh Rana, T. Ming Koh, D. Jun Jie Tay, A. Bruno, S. Mhaisalkar, N. Mathews, *ChemSusChem* **2021**, *14*, 1524.
[29] R. A. Kerner, S. Heo, K. Roh, K. Macmillan, B. W. Larson, B. P. Rand, *ACS Energy Lett.* **2021**, *6*, 501.
[30] S. Cacovich, L. Ciná, F. Matteocci, G. Divitini, P. A. Midgley, A. Di Carlo, C. Ducati, *Nanoscale* **2017**, *9*, 4700.

[31] X. Guo, T. M. Koh, B. Febriansyah, G. Han, S. Bhaumik, J. Li, N. F. Jamaludin, B. Ghosh, X. Chen, S. Mhaisalkar, N. Mathews, *ACS Appl. Mater. Interfaces* **2019**, *11*, 27882.
[32] J. P. Perdew, K. Burke, M. Ernzerhof, *Phys. Rev. Lett.* **1996**, *77*, 3865.
[33] H. J. Monkhorst, J. D. Pack, *Phys. Rev. B* **1976**, *13*, 5188.
[34] X. Liu, Z. Yu, T. Wang, K. L. Chiu, F. Lin, H. Gong, L. Ding, Y. Cheng, *Adv. Energy Mater.* **2020**, *10*, 2001958.
[35] C. Yi, J. Luo, S. Meloni, A. Boziki, N. Ashari-Astani, C. Grätzel, S. M. Zakeeruddin, U. Röthlisberger, M. Grätzel, *Energy Environ. Sci.* **2016**, *9*, 656.
[36] T. C. Sum, N. Mathews, G. Xing, S. S. Lim, W. K. Chong, D. Giovanni, H. A. Dewi, *Acc. Chem. Res.* **2016**, *49*, 294.
[37] S. S. Lim, D. Giovanni, Q. Zhang, A. Solanki, N. F. Jamaludin, J. W. M. Lim, N. Mathews, S. Mhaisalkar, M. S. Pshenichnikov, T. C. Sum, *Sci. Adv.* **2019**, *5*, eaax3620.
[38] J. W. M. Lim, D. Giovanni, M. Righetto, M. Feng, S. G. Mhaisalkar, N. Mathews, T. C. Sum, *J. Phys. Chem. Lett.* **2020**, *11*, 2743.
[39] J. Cao, S. X. Tao, P. A. Bobbert, C.-P. Wong, N. Zhao, *Adv. Mater.* **2018**, *30*, 1707350.
[40] X. Liu, Y. Zhang, L. Shi, Z. Liu, J. Huang, J. S. Yun, Y. Zeng, A. Pu, K. Sun, Z. Hameiri, J. A. Stride, J. Seidel, M. A. Green, X. Hao, *Adv. Energy Mater.* **2018**, *8*, 1800138.